Wrapping up : nidovirus membrane structures and innate immunity

Oudshoorn, D.

Chapter 3

New insights in the biogenesis of arterivirus replication organelles

Diede Oudshoorn[1], Barbara van der Hoeven[1], Abraham J. Koster, Eric J. Snijder , Marjolein Kikkert and Montserrat Bárcena

[1] These authors contributed equally to this study

The contents of this chapter were published, in modified form, as part of the review "Biogenesis and architecture of arterivirus replication organelles." (Virus Res. 2016 Jul 15;220:70-90) by B. van der Hoeven, D. Oudshoorn, A.J. Koster, E.J. Snijder, M. Kikkert and M. Bárcena.

ABSTRACT

All positive-strand RNA (+RNA) viruses of eukaryotes modify cellular membranes into replication organelles to facilitate their replication. The most prominent replication-associated membrane structures induced in cells infected with nidoviruses (including arteri- and coronaviruses) are double-membrane vesicles (DMVs). Using the equine arteritis virus (EAV) model for nidovirus replication and electron tomography, we obtained new data regarding the biogenesis of arterivirus-induced DMVs and uncovered numerous putative intermediates in DMV formation. We generated cell lines that can be induced to express specific EAV replicase proteins and showed expression of the transmembrane proteins nsp2 and nsp3 induced the formation of DMVs that constitute a reticulovesicular network (RVN) and are comparable in terms of architecture to those formed during viral infection. Co-expression of the third EAV transmembrane protein (nsp5), expressed as part of a self-cleaving polypeptide that mimicked viral polyprotein processing in infected cells, led to the formation of DMVs whose size was more homogenous and closer to what is observed upon EAV infection, suggesting a regulatory role for nsp5 in modulating membrane curvature and DMV formation.

INTRODUCTION

Double-membrane vesicles (DMVs) are the most prominent membrane structures formed upon nidovirus infection. However, the process of DMV biogenesis is still poorly understood. DMV biogenesis is mechanistically complex, probably involving a defined sequence of events (see **Chapter 2**) and multiple players including the membrane donor organelle (the endoplasmic reticulum in the case of nidoviruses), host protein factors involved and viral proteins required (discussed below). Unraveling the different stages of membrane transformation, and the underlying molecular interactions, will be essential for a full understanding of arterivirus DMV biogenesis. Addressing some of these questions in the context of virus-infected cells is complicated by the (potential) number of viral players involved and the fact that targeting the viral proteins with mutagenesis often leads to defects that inhibit or block viral replication. The development of so-called "surrogate systems for DMV formation", however, does create the possibility to address these questions by essentially uncoupling the expression of the viral proteins under study from their expression from a viable viral genome. In such systems, ectopic expression of a subset of viral proteins is used to mimic the formation of membrane structures that resemble those found during infection, although they obviously lack the viral RNA-synthesizing enzyme complexes associated with these structures in infected cells. For a number of viruses this approach has proven to be productive and, in many cases, instrumental for a better understanding of the biogenesis of virus-induced replication organelles (23-28, 38, 39). These systems can be expanded by using site-directed mutagenesis of the proteins that are expressed in order to probe the relevance of specific residues, protein domains or interactions.

For EAV, this approach has been instrumental in the identification of the proteins that are likely driving the conversion of specific intracellular membranes into viral replication organelles. Initially, the expression of EAV nsp2-7 in BHK-21 cells was shown to give rise to membrane rearrangements that were similar to those found in infected cells (88). The minimal set of viral proteins required for DMV formation was later narrowed down to nsp2 and nsp3 (24) and, since then, expression of these two proteins has been considered a useful surrogate system to mimic and study EAV-induced membrane modifications. Although these studies highlighted the key role of EAV nsp2 and nsp3 in DMV formation, the ultrastructural analysis was limited to 2D electron microscopy of chemically fixed samples. Therefore, the question of whether the detailed architecture of the DMVs induced upon co-expression of nsp2 and nsp3 was comparable to that of the DMVs found in infected cells remained unanswered. Furthermore, although nsp2 and nsp3 were shown to suffice to induce DMV formation, it was unknown whether the third transmembrane protein (nsp5) plays a role during arterivirus DMV biogenesis. In order to address these questions, we now carried out an electron tomographic characterization of the structures induced by different combinations of EAV-encoded non-structural proteins using two protein expression systems and samples prepared by high-pressure freezing (HPF) followed by freeze substitution (FS).

Clear intermediate structures that could support or argue against one of two models for arterivirus-induced DMV biogenesis (described in **Chapter 2**, Fig. 5) have not been visualized so far. Historically, the so-called enwrapping model has been favored due to the detection of short stretches of tightly paired membranes (88, 112), which could constitute a specific feature of this mechanism. Using ET on EAV-infected cells, we now found several intermediates compatible with either of the (non-mutually exclusive) DMV biogenesis models. The particularly frequent observation of tightly paired ER membranes suggests that enwrapping is at least a key process of DMV biogenesis.

RESULTS & DISCUSSION

Expression of EAV nsp2-3 using a Sindbis virus-based vector

We first analyzed the membrane modifications induced by EAV nsp2 and nsp3 using a Sindbis virus-based expression system, essentially identical to that used in previous studies in BHK-21 cells (24, 89). Alphaviruses like Sindbis virus also alter cellular membranes (see **Chapter 2**); however, they modify endosomes, lysosomes and the plasma membrane (59, 61, 157) and therefore are thought not to interfere with arterivirus-induced DMV formation. The system consisted of an RNA replicon (SINrep5) in which a foreign gene (a self-cleaving EAV nsp2-3 polypeptide C-terminally fused to enhanced GFP (eGFP)) replaced the ORF encoding the structural polyprotein of Sindbis virus and was expressed to high levels from a subgenomic mRNA (158). The eGFP tag on nsp3 enabled the application of correlative light and electron microscopy (CLEM), an emerging methodology that allows imaging of the same sample both by light microscopy and high-resolution EM (159). In order to carry out CLEM, we used a freeze-substitution protocol that minimizes staining to preserve the fluorescence throughout EM sample preparation (160). The eGFP signal facilitated the quick identification of transfected cells and, more specifically, the localization of nsp3-eGFP positive sites in the EM sections (Fig. 1A-C). In all these areas, some circular double-membrane profiles typical of DMVs were readily observed (Fig. 1C, white asterisks).

Intriguingly, numerous irregular structures that were also delineated by two tightly apposed membranes were readily apparent in the regions containing membrane modifications (Fig. 1C, black arrows). Electron tomography revealed that this type of irregular structures consists of strikingly long stretches of paired membrane sheets (Fig. 1D, black arrows) which appear to derive from the ER, with which they are continuous (Fig. 1E,F). Although the majority of the circular double-membrane profiles observed in 2D projection images were found to be closed DMVs upon tomographic analysis (Fig. 1D, white arrow) and thus analogous to those found in EAV infection, many apparent DMVs turned out to be patches of these membrane sheets that locally curved creating a secluded internal space reminiscent of a DMV but still continuous with the cytosol (Fig. 1G). In fact, these DMV-like structures, which could be easily mistaken for bona fide DMVs in 2D projection images, appeared to be part of a large network of double-membrane sheets weaving through the perinuclear area of the cytoplasm (Supplementary movie 2).

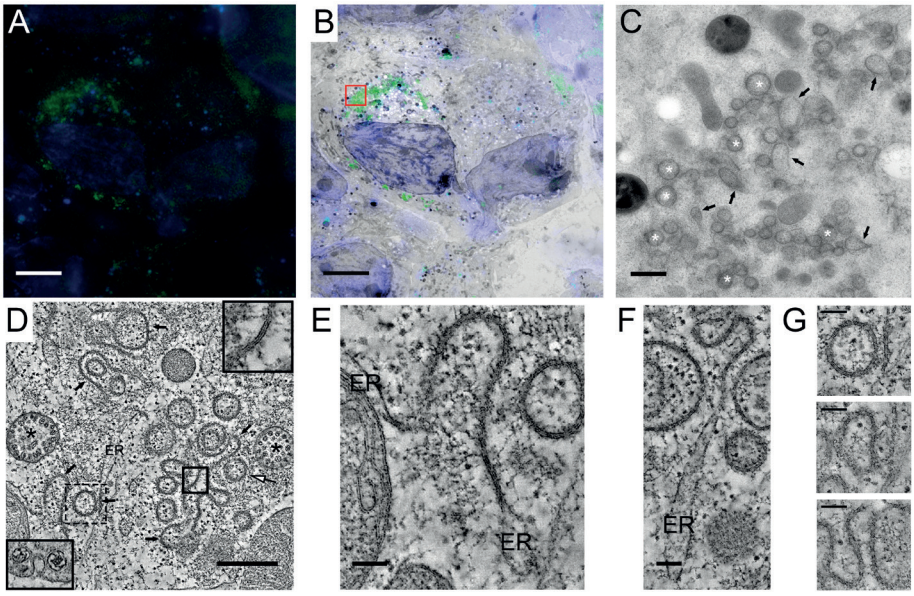

Fig. 1. Characterization of membrane structures induced by EAV nsp2-3 expression from a Sindbis virus-based replicon. (A-C) *Correlative light-electron microscopy (CLEM) analysis of transfected cells expressing an eGFP-tagged self-cleaving nsp2-3 polyprotein.* **(A)** *Fluorescence microscopy image of a 200 nm section on an EM grid showing nuclear DNA staining and a clear cytosolic eGFP signal.* **(B)** *Merging of the fluorescence image and the corresponding electron microscope images.* **(C)** *Higher magnification image of the boxed area in panel B, showing the structures underlying the eGFP signal. Several circular profiles typical of DMVs are clearly visible (white asterisks), as well as other more irregular double-membrane structures (black arrows).* **(D-G)** *3D architecture of nsp2-3 induced membrane rearrangements.* **(D)** *Tomographic slice (2 nm thick) of EAV nsp2-3-induced structures (see also Supplementary movie S2). These consist of the characteristic double-membrane vesicles (white arrow), as well as double-membrane sheets (black arrows) that are particularly abundant in this region. The membrane structures induced by Sindbis non-structural proteins are also visible (black asterisks), and consist of invaginations in modified endosomes that have a neck-like channel connecting their interior with the cytosol, (lower left inset). The inset at the upper right corner is a close-up of the boxed area in (D) (continuous line) and highlights the two tightly-apposed membranes that form these structures.* **(E,F)** *Gallery of tomographic slices (6 nm thick) highlighting the continuity of the paired-membrane sheets with ER cisternae.* **(G)** *Tomographic slices through the structure highlighted in (D) with a dashed box (relative z height of the slices, from top to bottom: 0, 35 and 60 nm). Notice how at one level (top image) the structure appears indistinguishable from a closed DMV, while the successive tomographic slices reveal that it is actually open to the cytosol and more akin to a highly curved fragment of the paired membrane sheet network to which it is connected. Scale bars, 10 µm (A-B), 500 nm (C-D); 100 nm (E-G).*

Movie S2 *(available at http://www.sciencedirect.com/science/article/pii/S016817021630199X). Tomography of the membrane structures induced by nsp2-3-eGFP expression from a SINrep5 replicon in HuH-7 cells. The movie shows consecutive slices (1.2 nm thick) through the reconstruction of the area displayed in Fig. 1D.*

This profusion of membrane sheets is a phenomenon that had been described before in the SINrep5nsp2-3 expression system, but only when a mutation creating an N-linked glycosylation site was introduced in the first luminal loop of nsp3 (T873N) (89) and not in cells expressing wild-type EAV nsp2-3 (24, 89). The reasons for this discrepancy are unclear and, although it may be partially attributed to the lack of 3D data in previous studies, it could also be related to differences in the experimental set-up. In any case, these differences were not related to the cell line used, nor were they due to the eGFP tag on nsp3 since similar double-membrane sheet networks were detected using BHK-21 and Vero E6 cells and the same construct lacking the eGFP fluorescent tag (data not shown).

Cell lines for the inducible expression of EAV nsps2-3 and nsp2-7

In order to avoid possible undesired side-effects derived from the expression of Sindbis virus non-structural proteins and to obtain a surrogate system that is more convenient, reproducible and suitable for a wider range of experimental setups, we created stable cell lines which can be induced to express the self-cleaving EAV nsp2-3 polyprotein from a cytomegalovirus (CMV) promoter.

Clusters of DMVs were readily observed 24 hours after induction of expression in HuH-7 cells (Fig. 2A, white asterisks). Both the inner and outer membranes of these DMVs were decorated with ribosomes (Fig. 2B,C, black arrows), which, as in the infected cell, hints at the ER as the membrane donor for DMV formation. In fact, some of these DMVs showed a direct connection with ER cisternae, with which they were continuous through their outer membrane (Fig. 2D). As in the case of DMVs found in infected cells, neck-like membrane connections between DMVs were detected in the tomograms (Fig. 2E, black arrowheads). Finally, the similarities with DMVs observed in EAV infection extended to the closed nature of these compartments, as no openings could be detected in the DMVs induced by nsp2-3 expression in this system.

Despite these general similarities, some anticipated differences with the structures found in infected cells were apparent. No tubular proteinaceous structures (**Chapter 2**; Fig. 2H,I) were detected, which is in agreement with the notion that their formation depends on N protein expression (20, 115). Also, the DMVs formed upon expression of nsp2-3 lack the electron dense core that is typical of the DMVs in EAV-infected cells. The absence of this structure is consistent with the interpretation that the DMV cores that appear in infected cells, which have a high phosphorus content and label for dsRNA (**Chapter 2**; Fig. 3), contain viral RNA. The content of the nsp2-3-induced DMVs appears quite similar to the surrounding cytosolic material, although slightly more electron dense and, like the cytosol, it contains densities that may be free ribosomes (Fig. 2D,E white circles). Taken together, our results show that the expression of nsp2-3 suffices to reproduce the double-membrane architecture, topology and connectivity of the DMVs found in infected cells, and therefore constitutes a useful system to study these features of the EAV-induced RVN. This also implies that the membrane-remodeling capacities necessary to generate the RVN reside in these two arteriviral nsps, likely with the assistance of recruited host factors.

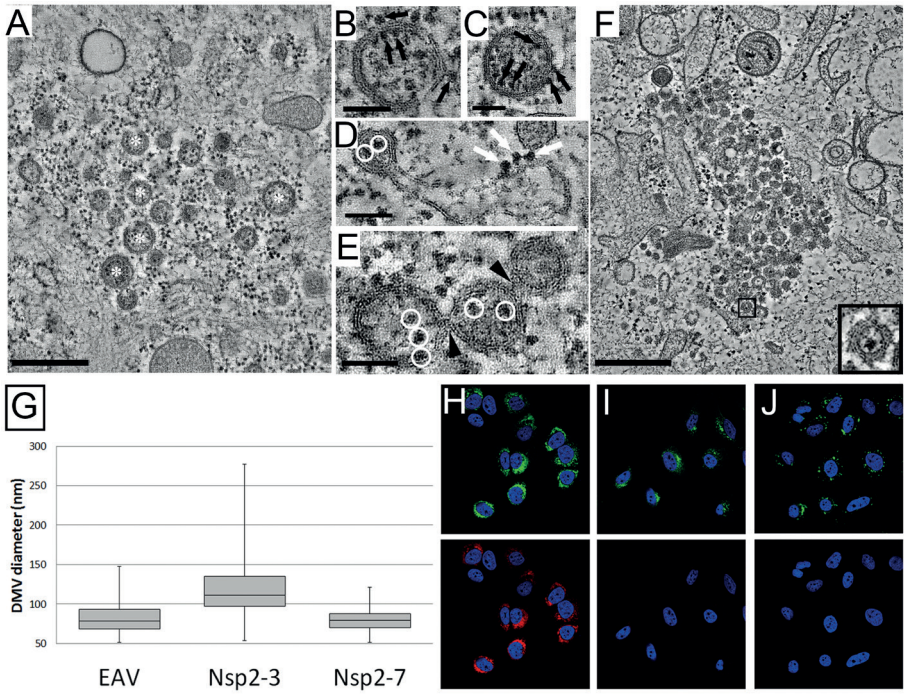

Fig. 2. Characterization of membrane structures induced after EAV nsp2-3 and nsp2-7 expression using inducible HuH-7 cell lines. (A) *Tomogram slice (2 nm thick) showing an overview of the structures induced upon nsp2-3 expression. The structures consist of DMVs, some of which are indicated by white asterisks. Note that the membrane sheet network observed in the SINrep5 expression system (Fig. 7) is absent.* **(B-E)** *Close-up tomographic slices (6 nm thick) highlighting several features of the DMVs induced by nsp2-3 expression.* **(B,C)** *Ribosomes decorate both the inside and the outside of the DMVs (black arrows).* **(D)** *An example of membrane continuity between rough ER and DMV, similar to what is found for DMVs induced in EAV infection (Fig. 2B). The ribosomes decorating the surface of the ER membrane are indicated by white arrows, while the ribosomes in the interior of the vesicle are encircled in white. Another feature, highlighted in* **(E)**, *is the propensity for the DMV to form interconnections similar to those found in EAV-induced DMVs (black arrowheads).* **(F)** *Virtual slice (2 nm thick) showing an overview of the typical structures seen upon induction of nsp2-7 expression, which consist of clusters of DMVs. The inset shows a close-up of the DMV in the boxed area, which appears to contain a ribosome.* **(G)** *Boxplot illustrating the diameter distribution for DMVs induced by EAV infection, nsp2-3 expression and nsp2-7 expression in HuH-7 cells, as measured from the tomographic reconstructions from samples prepared in parallel in the same experiment. The middle of the boxplot represents the median value for each population, the bottom and top of the boxplot represent the first and third quartile respectively. The whiskers extend to the minimum and maximum measured values.* **(H-J)** *Immunofluorescence labeling of viral markers in EAV-infected HuH-7 cells (H) and in the inducible HuH-7 cell lines expressing nsp2-3 (I) or nsp2-7 (J). A perinuclear nsp2 labeling (top, green) was apparent in the three experimental conditions, while dsRNA signal (bottom, red) was only detected in EAV-infected cells. Scale bars, 500 nm (A,I); 100 nm (B-E).*

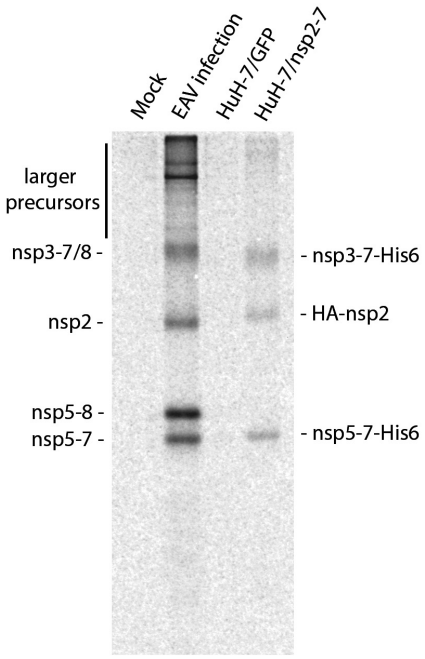

Fig. 3. Figure comparing the polyprotein processing during EAV infection and in HuH-7/tetR/nsp2-7 cells. *EAV infected and mock HuH-7 cells as well as HuH-7/tetR/nsp2-7 cells and control HuH-7/tetR/eGFP were metabolically labeled with 100 µCi/mL 35S methionine and 35S cysteine (EXPRE35S35S Protein Labeling Mix; Perkin-Elmer) for 4-10 hours post infection or tetracycline induction. Immunoprecipitation was performed as described previously with an antiserum raised for amino acids 1508-1727 (nsp7-8) of pp1a (134). Cleavage products observed during EAV infection are indicated on the left side and for nsp2-7 expressing cells on the right side.*

The results with this nsp2-3 expression system raise the question of the role in DMV formation, if any, of the third (presumed) transmembrane subunit of the arterivirus replicase: nsp5. To investigate this, using the same approach as above, we created a stable inducible HuH-7 cell line expressing nsp2-7. Since most nsp5 molecules in infected cells are present in the form of nsp5-7 or nsp5-8 processing intermediates (77, 84), expression of a self-cleaving nsp2-7 was chosen to mimic the course of events in infected cells most closely (Fig. 3). As in the case of nsp2-3, induction of nsp2-7 expression gave rise to the appearance of DMV clusters in close proximity to the ER (Fig. 2F). Notably, these DMVs observed in HuH-7 cells at 24 h after induction were strikingly smaller than those observed upon expression of nsp2 and nsp3 only. A detailed DMV size comparison was carried out using the 3D-reconstructions (Fig. 2G, Table 1). This method provides a much more reliable estimate of vesicle sizes than 2D measurements because, inevitably, not every DMV is fully contained in a cell section. Only a 3D analysis allows exclusion of DMVs whose equator is not present in the cell section. In this manner, the average diameter of the nsp2-7-induced DMVs was determined to be 79 nm (±13 nm, n=145) versus 119 nm (±32 nm, n=145) for nsp2-3-induced DMVs. The average size difference between the two populations, which translates into a decrease in DMV volume of about 70%, was found to be statistically significant using an independent two-sample *t*-test (Table 1). Remarkably, expression of nsp2-7 seems to bring the average diameter of the DMVs closer to the average diameter of DMVs formed in EAV infection (83 ±21 nm, n=145). Additionally, the population of nsp2-7-induced DMVs appeared to be significantly more homogenous in size than the DMVs

	n	Median	Average	Standard deviation	p-value[a]	p-value[b]	p-value[c]
EAV infection	145	78	83	21	-	<0.001	<0.05
Nsp2-3	145	111	119	32	<0.001	-	<0.001
Nsp2-7	145	80	79	13	<0.05	<0.001	-

Table 1. Diameters of DMVs in EAV infection, nsp2-3 expression and nsp2-7 expression.

[a] *Comparison with diameters of DMVs formed upon EAV infection.*

[b] *Comparison with diameters of DMVs formed upon nsp2-3 expression.*

[c] *Comparison with diameters of DMVs formed upon nsp2-7 expression.*

produced upon expression of just nsp2 and nsp3, where particularly large DMVs (up to ~270 nm in diameter) were detected (Fig. 2G). The DMVs in the nsp2-7-expressing cell line also lacked the electron dense core typical of DMVs formed upon EAV infection, although their content appeared slightly more electron dense than the surrounding cytosolic material. The dark content often seemed to correlate with the presence of densities that resembled ribosomes (Fig. 2F, inset). In any case, immunofluorescence microscopy confirmed that this darker interior is not due to the presence of dsRNA. As expected for systems lacking viral RNA replication, no dsRNA signal could be detected in cells expressing either nsp2-3 or nsp2-7, in contrast with the abundant dsRNA labeling found in EAV-infected HuH-7 cells (Fig. 2H,I,J).

Overall, our results show that, while nsp2 and nsp3 are capable of inducing all the membrane-remodeling steps required to generate the virus-induced RVN, the presence of additional nsps can modulate the process and produce DMVs more similar in size to those found in EAV-infected cells. The significantly smaller DMVs found upon nsp2-7 expression relative to those induced by nsp2-3 suggest a role for the extra proteins in enhancing the curvature of the membranes used for DMV formation, while the narrower size distribution suggests a tighter regulation of the process. Although several additional nsps and intermediates are expressed in the nsp2-7 system, it seems likely that, nsp5, given its presumed transmembrane nature, is the primary cause of the observed differences.

Comparison with the role of coronavirus nsps in membrane remodeling

In terms of host cell membrane remodeling, the coronaviral non-structural proteins 3, 4 and 6 that contain three conserved transmembrane domains (TM1, TM2 and TM3) are considered to be the functional equivalents of arterivirus nsp2, nsp3 and nsp5, respectively (78). A recent study addressed the question of the membrane-remodeling abilities of the SARS-CoV proteins nsp3, nsp4 and nsp6, using (co-)transfection of plasmids encoding separate nsps to express them either individually or in various combinations, followed by an ultrastructural analysis of the cells by EM (28). In this experimental set-up, co-expression of these three nsps appeared to be required for the formation not only of DMVs but also of structures resembling the CM that are typical of SARS-CoV infection (**Chapter 2**; Fig. 4B). This outcome differs from the results obtained with arteriviruses, where expression of

just nsp2 and nsp3 was sufficient, as described above, for the formation of closed DMVs in the expression systems tested. The corresponding combination of coronavirus nsps, namely SARS-CoV nsp3 and nsp4, gave rise to membrane structures termed maze-like bodies, which consisted of clusters of curved parallel-running profiles of ER-derived paired membranes (28). Interestingly, these were interspersed with circular profiles delineated by a double membrane. The circular profiles had an average diameter similar to the average spacing of the curved parallel double-membrane profiles (~80 nm), and they were interpreted, respectively, as cross or longitudinal sections of double-membrane walled tubules. However, in the absence of 3D-EM data, the authors recognized that is was not possible to firmly establish this point. In our opinion, the circular double-membrane profiles may alternatively represent DMVs interspersed with regions of paired membranes sheets, similar to what is observed upon expression of EAV nsp2-3 in the Sindbis virus-based expression system (Fig. 1). This is a particularly interesting possibility as it would imply that, both for arteriviruses and coronaviruses, the proteins containing TM1 and TM2 would be sufficient to induce DMV formation. In this alternative scenario, the nsp comprising TM3 may merely have a modulating role in DMV formation and, in coronaviruses, could be important for the generation of CM.

In any case, the presence of maze-like bodies reflects that expression of coronavirus nsp3 in combination with nsp4 is able to induce membrane-pairing, which is likely an essential step in DMV formation. The membrane pairing observed in the maze-like bodies appeared to strictly depend on the co-expression of nsp3 and nsp4, suggesting that it could be the result of heterotypic interactions between these proteins (28). This type of interaction between nsp3 and nsp4 has been biochemically detected by mammalian two-hybrid assay (161) and co-immunoprecipitation (162), and may resemble the nsp2-nsp3 interaction documented for arteriviruses (89, 134).

Additional experiments provided some interesting hints regarding the specific domains that could be important for the nsp3-nsp4 interaction possibly leading to membrane-pairing. The co-expression of MHV nsp4 and a C-terminal fragment of nsp3 that contained the two predicted transmembrane domains changed the localization of these proteins from the ER to discrete perinuclear foci (162). At the ultrastructural level, the two nsps mapped to regions of highly curved, ER-derived membranes that were vaguely reminiscent of the maze-like bodies described by Angelini *et al.* (2013) (96). Using truncated mutants, the critical regions for the relocation of these proteins to foci could be narrowed down to the luminal loop of nsp3 and the first luminal loop of nsp4 (96). This large N-terminal nsp4 loop contains ten conserved cysteines, which could be important in inter- or intra-molecular interactions. Mutations in each of these cysteines severely impaired the relocation of nsp4 and the nsp3 C-terminal fragment, suggesting an important direct or indirect role of these cysteines in the nsp3-nsp4 interaction (96). Like the coronavirus nsp4, the corresponding arterivirus protein (nsp3) contains a cluster of four conserved cysteine residues in its first luminal loop, and each of them appeared to be critical for DMV formation and virus replication (89). The latter study also showed, by mutating a catalytic residue in PLP2 (H332Y), that the cleavage between nsp2 and nsp3, although essential for virus replication, was dispensable for DMV

formation in an expression system. When expressed from the SINrep5 vector in BHK-21 cells, an nsp2-3 construct containing an N glycosylation site in the cysteine-containing loop induced the abundant formation of curved paired membranes, which was interpreted as partial inhibition of DMV formation (89). These modifications, however, closely resemble the results now obtained using wild-type nsp2-3 expressed from a Sindbis virus-based vector and therefore perhaps reflect peculiarities of this expression system rather than an effect of the mutation. This latter possibility seems to be supported by preliminary results for this mutant when expressed in an inducible HuH-7 cell line, in which long curved paired membranes could not be detected whereas regular DMV clusters were present (data not shown).

One major difference between studies on coronaviruses and arteriviruses (24, 88, 89), is that coronavirus nsps were expressed independently from separate plasmids, whereas arterivirus proteins were expressed as (more natural) self-cleaving polyproteins. Obviously, the former poorly mimics the situation in infected cells and could influence the course of events during which translation, polyprotein cleavage, nsp translocation, and membrane remodeling occur, likely in a defined order. Also processing intermediates could play an important role in membrane rearrangement, for example, by keeping nsps in close proximity to each other to favor key interactions in the membrane remodeling process. Additionally, it should be noted that proteins made from polyproteins are produced at equimolar ratios, something that is virtually impossible to control when co-transfecting multiple plasmids. Unfortunately, the exceptionally large size of coronavirus nsp3 (~2000 amino acids long) has so far complicated the production of the nsps from a self-cleaving polyprotein in an expression system. Future studies that overcome this technical difficulty may be pivotal to definitively establish the similarities and differences between coronaviruses and arteriviruses regarding the membrane-remodeling abilities of their nsps.

Intermediates of DMV biogenesis

We now have performed an extensive tomographic analysis that uncovered the 3D structure of some distinct intermediates that further support an enwrapping mechanism for DMV formation. These intermediates (observed in EAV-infected HuH-7 cells) include relatively long stretches of paired ER membranes that represent sheets according to the 3D analysis and could reflect the first step in DMV formation through enwrapping (Fig. 4A). In order to transform these sheets into DMVs, curvature must be induced and paired-membrane sheets with different degrees of curvature could indeed be detected in the tomograms (Fig. 4B). A (putative) even more advanced stage, in which the paired curved sheet is already transformed into a nascent DMV that is not yet completely sealed, is shown in Fig. 4C,D.

Given the similarities between arterivirus- and coronavirus-induced DMVs and the presumed common ancestry of their replicase proteins, including the subunits likely to drive the membrane modifications, it is tempting to speculate that the enwrapping mechanism could also be used for the formation of DMVs in coronavirus infection. In this regard, there are some striking similarities between the intermediate paired-membrane structures shown here for EAV and the zippered ER membranes recently documented for

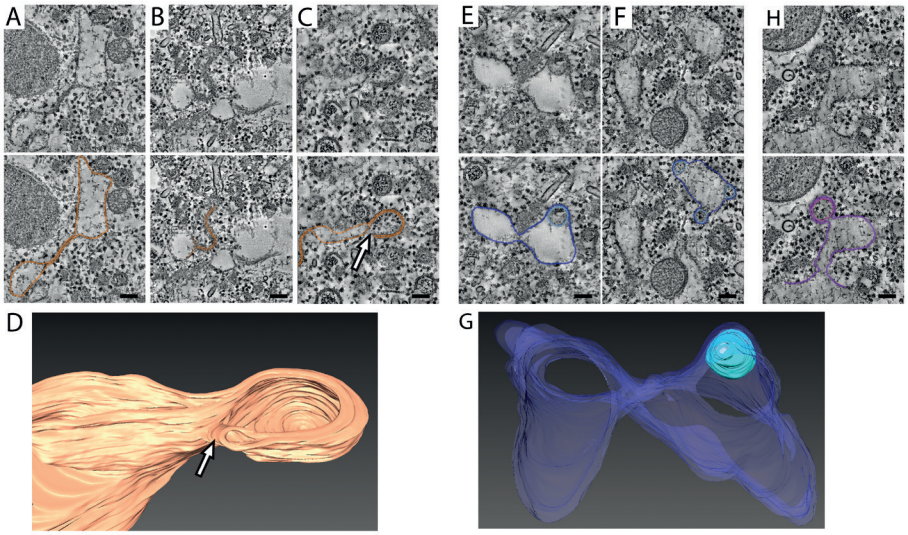

Fig. 4. Putative intermediate structures in the formation of DMVs. *The grayscale top images are virtual slices (6 nm thick) extracted from tomograms of EAV-infected HuH-7 cells.* **(A-C)** *Putative intermediates of an enwrapping process. The membranes of interest are highlighted in orange in the lower images. (A) Paired ER membranes, possibly corresponding to the stage sketched in* **Chapter 2** *Fig. 5A as II. This type of paired membranes could progressively curve (B) to form a vase-like double-membrane compartment (C, D) (stage represented in* **Chapter 2***; Fig.5A as III) with an opening to the cytosol (white arrows).* **(D)** *3D-surface rendering of the structure shown in panel C.* **(E-F)** *Structures compatible with intermediates in a double-budding mechanism. In the lower panels, the membranes are highlighted in dark blue (ER) and light blue (luminal vesicle). These structures could represent a stage between III and IV in* **Chapter 2***; Fig.5B, in which a luminal vesicle interacts with an ER membrane that curves towards the cytosol, possibly to form the outer membrane of a nascent DMV.* **(G)** *3D surface-rendered model of the structure shown in panel E.* **(H)** *Example of a DMV that is connected to the ER though it lacks the electron dense core usually seen in DMVs. The membranes are highlighted with purple (ER membranes) and pink (inner vesicle). Scale bars, 100 nm.*

the gammacoronavirus IBV (**Chapter 2**; Fig. 4C). These zippered membranes also appear to curve, forming open double-membrane spherules that, nevertheless, were ruled out as DMV precursor by Maier *et al.* due to their much smaller size (~60 nm in diameter versus ~180 nm for IBV DMVs) and their different appearance (22). Interestingly, the tomographic analysis of cells infected with the enteroviruses CVB3 and PV revealed putative intermediate structures supporting an enwrapping mechanism for the biogenesis of the DMVs induced by these viruses (56, 65). Taken together, these results suggest that enwrapping may well be a general route used for the generation of virus-induced DMVs.

Nevertheless, in our search for intermediates that could shed light on the biogenesis of EAV-induced DMVs, we also detected structures in infected HuH-7 cells that would be compatible with a double-budding mechanism. These consisted of sealed SMVs contained in the ER lumen and closely apposed to the ER membrane to possibly recruit the

second membrane through membrane pairing (Fig. 4E,F,G). We cannot discard, however, an alternative scenario in which these luminal SMVs would result from a distension of the connection between an already formed DMV and the ER. Although the putative double-budding intermediates were considerably rarer in our tomograms than the structures that would fit with the enwrapping model, this lower frequency cannot be directly translated into a quantitative assessment about the prevalence of the two mechanisms, as it could simply reflect that double-budding is a faster process that is therefore under-represented in the snapshots that EM provides. Overall, our data suggests that the enwrapping mechanism plays an important role in DMV formation but is also compatible with a model in which both enwrapping and double-budding would coexist. In this regard, it is interesting to emphasize that the fundamental difference between the two proposed mechanisms is simply the order in which essentially the same membrane reshaping events would take place (**Chapter 2**; Fig. 5). It is therefore conceivable that, having the molecular mechanism required for these steps in place, both paths could be used by the virus for the ultimate goal of forming DMVs.

An interesting feature of all putative nascent DMVs observed in the tomograms (Fig. 4C,E,F) is that they lack the electron-dense core that is typical of most DMVs found in EAV infected cells. However, occasionally fully-formed DMVs that do not contain such a core could also be detected. DMVs lacking and containing a core are indistinguishable in size and both types often appear to be connected to the ER (Fig. 4H). In our view, they could well represent early and later stages in the existence of a DMV. In this scenario, the DMV content would be initially identical to the surrounding cytosolic material. Once fully formed and closed, the DMV would accumulate electron-dense material. The exact nature of this material remains unclear although one of its components must be dsRNA.

CONCLUSIONS AND FUTURE PERSPECTIVES

The biogenesis of the DMVs formed upon nidovirus infection is an aspect that we are just beginning to address. The results presented here for EAV document clear putative intermediates in DMV formation by enwrapping of paired ER membranes as well as structures also compatible with a double-budding mechanism. This suggests that, maybe more than a strict sequence of events, the virus could "direct" basic membrane remodeling events (e.g. membrane pairing and induction of membrane curvature) that could be used in different routes ultimately leading to the same (or similar) structures. Viral proteins are likely to drive RVN biogenesis with the aid of host factors that, in the case of nidoviruses, remain to be identified. It seems clear now that both in arteri- and coronaviruses the TM1- and TM2-containing nsps are sufficient to produce membrane pairing (24, 28) and, in arteriviruses, also suffice for the formation of DMVs that have a comparable architecture to those found in infection. Our results suggest that the TM3-containing nsp, which has been proposed to be essential for DMV formation in coronaviruses (28), would merely have a curvature-modulating role in DMV biogenesis in the case of arteriviruses. Similar electron tomography studies with coronaviral nsp expression systems may help to firmly establish the similarities

and differences between arterivirus- and coronavirus-induced DMV formation. This kind of 3D-ultrastructural studies, possibly complemented with similar analyses *in vitro* using membrane model systems (163), could be a significant step towards the mechanistic dissection of the role of the nsps and their different domains in RVN biogenesis.

The stable inducible cell lines ectopically expressing EAV nsps that we present in this study, besides closely mimicking the morphology of DMVs in EAV-infected cells, open multiple possibilities for future research. These 'surrogate systems', inducibly expressing self-cleaving nsp constructs, could be employed, for example, to investigate the interplay between the virus-induced membrane structures and different host factors and pathways (e.g. innate immunity, autophagy), to study how viral proteins affect cellular lipid homeostasis, as well as in the search for new antiviral drugs that specifically target viral replication organelles.

Acknowledgements

We thank Ronald Limpens for general technical assistance and discussions. This work was supported in part by the Netherlands Organization for Scientific Research through a TOP grant from the Council for Chemical Sciences (NWO-CW grant 700.57.301 to EJS and AJK) and a MEERVOUD grant (NWO-ALW grant 836.10.003 to MB) from the Council for Earth and Life Sciences.

MATERIALS AND METHODS

Cells, virus, and infections

HuH-7 cells were cultured in Dulbecco's modified Eagle's medium supplemented with 8% fetal calf serum, non-essential amino acids (PAA), L-glutamine (PAA)), and penicillin/streptomycin (PAA). Cells were infected with a cell-culture-adapted EAV Bucyrus isolate (5). Infections were carried out with a multiplicity of infection of 10 and incubated at 37°C for 12 h before further processing.

Construction of EAV expression vectors

EAV polyprotein constructs were assembled in pDONR201 (Invitrogen) based on the previously described full-length cDNA clone of EAV pEAN511(89). Constructs for the expression of nsp2 and nsp3 contained amino acids 261-1063 of EAV pp1a with an HA-tag fused to the N-terminus of nsp2. The C-terminus of nsp3 lacked the final glutamic acid of nsp3 and was instead fused to either a His6 tag or enhanced GFP (eGFP). Polyprotein constructs of EAV pp1a nsp2-7 (amino acids 261-1676, lacking the last glutamic acid of nsp7) were fused to an HA-tag at the N-terminus and His6 tag at the C-terminus. Using gateway cloning, polyprotein constructs, as well as eGFP controls, were shuttled to either a modified Sindbis replicon vector based on SINrep5 (158) in which a gateway cassette was inserted into the multiple cloning site (pSR5-DEST) or the lentivirus vector pLenti6.3/TO/V5-DEST (Invitrogen).

Transfections

pSR5 constructs were linearized with XhoI followed by *in vitro* RNA synthesis using a SP6 mMESSAGE mMACHINE kit (Thermo). Cells were transfected using AMAXA electroporation with 1 µg SR5 RNA for each 1x106 cells and incubated at 37°C for 24 hours until analysis.

Generation of stable inducible cell lines

Lentivirus particles of pLenti6.3 constructs and pLenti3.3/tetR (Invitrogen) were generated as described previously (136). HuH-7 cells were transduced first with Lenti3.3/tetR lentivirus particles and selected using 500 µg/ml G418 (PAA) to insert the tetR gene for tetracycline-regulated expression (164). After complete selection cells were transduced again with different Lenti6.3 constructs and selected using 12.5 µg/ml Blasticidin-S (PAA). Expression of recombinant EAV constructs was induced for 24 hours using 1µg/ml tetracycline (Invitrogen) prior to fixation and further analysis.

Immunofluorescence and light microscopy

Cells were fixed at indicated time points with 3% paraformaldehyde in a phosphate-buffered saline (PBS) solution, permeabilized with 0.1% Triton X-100 in PBS and then immunolabeled with nsp2-specific rabbit antisera (previously described in (165)) and a mouse monoclonal antibody specific for dsRNA (MAb J2) (166, 167). These were detected, respectively, using a goat anti-rabbit immunoglobulin conjugated to Alexa Fluor 488 and a donkey anti-mouse immunoglobulin conjugated to a Cy3 fluorophore (Jackson). Imaging was done using a Leica SP8 confocal laser scanning microscope, which was equipped with a 63x objective (NA 1.40; 1 Airy Unit) and a Leica HyD hybrid detector.

Electron microscopy sample preparation

HuH-7 cells grown on sapphire discs (Leica) were either infected with EAV, transfected with Sindbis virus replicons or, in the case of the transduced HuH-7 cell lines, induced to express EAV nsp constructs as described above and subsequently high-pressure frozen with a Leica EM PACT2 and freeze-substituted as previously described (20) using an AFS2 (Leica) equipped with a freeze substitution processor robot. The freeze substitution medium consisted of 2% osmium tetroxide, 1% glutaraldehyde and 10% H2O in acetone. The samples were then kept at -90°C for 9h after which the temperature was raised by 23.33°C/h to -20°C. This temperature was kept for 1 h after which the temperature was again raised by -20°C/h to 0°C. After 1 h at this temperature the samples were washed first with cooled down acetone and again at room temperature. The samples were then embedded in epoxy LX-112 resin and polymerized at 60°C for 48 h.

For CLEM samples, the freeze substitution method described by (160, 168) was used to preserve the eGFP signal. Samples were maintained at a temperature of -90°C in 0.1% uranyl acetate in acetone for 48h. The temperature was then raised by 5°C/h to -45°C at which point the samples were washed with acetone and resin infiltration was started by adding increasing concentrations of Lowicryl (Polysciences, Inc., USA) in acetone (10, 25, 50 and 75%) that were kept on the sample for 4 h each, while the temperature was slowly

raised to -25°C. The 75% Lowicryl in acetone was then exchanged with 100% Lowicryl in three infiltration steps of 10 h each. Polymerization by ultra-violet (UV) light was started -25°C and maintained for 48 h. The temperature was then raised 5°C/h to 20°C. UV light illumination was then maintained for an additional 48 h.

For all the samples, 200 nm sections were cut with a UC6 ultramicrotome (Leica). The sections for CLEM were picked up on finder grids coated only with carbon (F1 200 mesh, Electron Microscopy Sciences). Parallel bar copper grids (R100, Electron Microscopy Sciences) covered with a carbon-coated formvar layer were used for tomography samples, which were then additionally counter-stained by incubating the grids with uranyl acetate (120 min) and lead citrate (10 min).

Electron microscopy and electron tomography

EM data was collected on FEI Tecnai12 BioTWIN and TWIN microscopes operated at 120kV and equipped with Eagle 4k cooled slow-scan charge couple device (CCD) cameras. Grids for tomography were inserted into a dual-axis tomography holder (Fischione). SerialEM (169) and Xplore3D (FEI company) acquisition software packages were used to collect images covering 130° around the specimen in 1° increments around two perpendicular axes. The pixel size at the specimen level was 1.2 nm (BioTWIN data) or 1 nm (TWIN data). Alignment of the tilt-series and tomogram reconstruction by weighted back-projection were done using IMOD software (170). The 3D surface renderings of the tomograms were manually generated using the AMIRA visualization software (FEI Visualization Sciences Group) using a Wacom tablet and pen.

Correlative light and electron microscopy (CLEM)

Grids containing sections for CLEM were incubated with a Hoechst 33342 solution for 15 minutes to stain the nucleus of the cells in order to aid with the correlations. The grids were then washed, dried and subsequently mounted on a glass-slide in a drop of water with the section side facing up. This was then covered with a coverslip to enable oil immersion imaging, which was performed with a DM 5500 wide-field microscope (Leica) equipped with a 40x (NA 1.25) objective and a photometrics Coolsnap HQ B/W camera. The position on the grid of the fluorescence images was logged by using the marks on the finder grid. After light microscopy imaging the grids were dismounted from the glass-slide, dried at room temperature and transferred to the EM, where the logged positions were traced back. The overlay of the fluorescent and EM images was made in Photoshop using the nuclei in both images as reference points.